Fusion cross sections and barrier distributions for $^{16}O + ^{70,72,73,74,76}Ge$ and $^{18}O + ^{74}Ge$ reactions at energies near and below the Coulomb barrier

Vijay,[1,*] Rishi Pal Chahal,[1] Manjeet Singh Gautam,[2,†] Sukhvinder Duhan,[3] and Hitender Khatri[4]

[1]*Department of Physics, Chaudhary Bansi Lal University, Bhiwani (Haryana) 127021, India*

[2]*Department of Physics, Government College Alewa, Jind (Haryana) 126102, India*

[3]*Department of Applied Sciences and Humanities, Set Jai Parkash Mukand Lal Institute of Engineering and Technology, Radaur, Yamunanagar (Haryana) 135133, India*

[4]*Department of Physics, Government College for Women, Gharaunda, Karnal (Haryana) 132114, India*

(Received 27 June 2020; revised 16 October 2020; accepted 21 December 2020; published 8 February 2021)

In this paper, we have investigated the sensitivity of fusion cross section and the barrier distribution data with respect to the choice of the potential parameters. To ascertain this, the fusion dynamics of $^{16}O + ^{70,72,73,74,76}Ge$ and $^{18}O + ^{74}Ge$ reactions at near and sub-barrier energies have been examined. In the present study, we have used the one-dimensional Wong formula, symmetric-asymmetric Gaussian barrier distribution (SAGBD) model, and coupled channel approach. For theoretical estimations, the Woods-Saxon form of nuclear potential has been adopted, and it has been found that both the fusion cross section and barrier distribution are quite sensitive to the choice of potential parameters in the entire range of incident energies. Calculations based on the Wong formula are significantly smaller than the sub-barrier fusion data, which has clearly suggested that the couplings to the nuclear structure's degrees of freedom of the colliding nuclei are needed to reproduce the experimental data. On the other hand, in the SAGBD model calculations the multidimensional character of nucleus-nucleus potential has been incorporated and it has reasonably recovered both the fusion cross-section data and the barrier distribution data of $^{16}O + ^{70,72,73,74,76}Ge$ and $^{18}O + ^{74}Ge$ reactions. In the SAGBD model, channel coupling parameter λ has been determined from barrier distribution and hence λ is related to the various channel coupling effects which have arisen because of the nuclear structure of the participating nuclei. The increase in λ with an increase in target isotopic mass has clearly indicated that there are shape transition effects in Ge isotopes, which change their shape from spherical symmetry to prolate deformed shape as one moves from ^{70}Ge to ^{76}Ge. Similarly, the percentage reduction of effective fusion barrier V_{CBRED} with respect to uncoupled Coulomb barrier has also shown an increasing trend with the increase in target isotopic mass. In order to confirm the shape transition effects, the coupled channel calculations have been performed by using the code CCFULL. The present coupled channel analysis has clearly pointed out the importance of nuclear structure degrees of freedom of participating nuclei in the sub-barrier region. Similar results have also been evident from SAGBD analysis. Hence the model predictions incorporate the contributions from vibrational excitations and/or static deformation in the fusion of $^{16}O + ^{70,72,73,74,76}Ge$ reactions. For the $^{18}O + ^{74}Ge$ reaction, the vibrational excitations along with the neutron transfer channel have led to larger sub-barrier fusion enhancement and their influences have been automatically included in the SAGBD calculations. Furthermore, $^{16}O + ^{76}Ge$ and $^{18}O + ^{74}Ge$ reactions have formed the same compound nucleus ^{92}Zr via different entrance channels. Their comparative study has indicated that the effect of the neutron transfer channel has dominated over the entrance channel mass asymmetry effects. In addition, the minimum value of χ^2 that has been obtained for the SAGBD calculations is consistent with that of the coupled channel calculations.

DOI: 10.1103/PhysRevC.103.024607

I. INTRODUCTION

The intrinsic degrees of freedom (DOF) and/or neutron transfer couplings of the interacting nuclei strongly affect heavy-ion interactions at energies in the sub-barrier domain [1–9]. The fusion process has been assumed to occur if colliding nuclei either penetrate or overcome the resultant barrier formed due to Coulomb, nuclear, and centrifugal terms. This in turn forms a heavier compound nucleus with the release of a tremendous amount of energy [9–14]. In this sense, the one-dimensional barrier penetration model (1-DBPM), wherein relative motion between fusing nuclei is assumed to be the only DOF, is one of the simplest models that can be used for the estimations of the fusion process. It has been widely accepted that the channel coupling effects are crucial in heavy-ion fusion reactions. In heavy-ion fusion dynamics at near and sub-barrier energies, a significant role is played by the nuclear structure of interacting nuclei like rotational states

*ghanghasvijay93@gmail.com

†gautammanjeet@gmail.com

 ©2021 American Physical Society

(deformed nucleus), vibrational modes (spherical nucleus), permanent ground state deformation, zero-point motion of nuclear surface, entrance channel mass asymmetry, neck formation, and/or particle transfer channels. From the existing literature, one can conclude that the coupling of one or more intrinsic DOF of the colliding nuclei with their relative motion enhances the fusion probability, which in turn enhances fusion cross sections around the Coulomb barrier. The couplings to intrinsic channels result in the splitting of the original barrier into barriers of different weights and heights, and subsequently produce larger fusion cross sections at sub-barrier energies [1,13,15–19]. The barrier distribution, which was introduced by Rowley *et al.* [20], can be obtained by taking a double derivative of $E_{c.m.}\sigma_F$ with respect to center of mass energy $E_{c.m.}$ and hence it acts as a blueprint of the type of coupling involved in the sub-barrier fusion enhancement. In this sense, the barrier distribution method is an effective tool to explore the role of intrinsic DOF in the fusion dynamics [1,16,17,21].

From the literature, one can easily understand that the choice of nucleus-nucleus potential is very crucial in describing the fusion reaction dynamics. The conventional Woods-Saxon potential (WSP) has been very popular and commonly used to explore the dynamics of heavy ion fusion reactions [13,22,23]. The WSP consists of three parameters, namely range, potential depth, and diffuseness, which are interrelated with each other. In the literature [15,16,19,24–30], it has been pointed out that an anomalously larger value of diffuseness parameter is needed to explore the sub-barrier fusion dynamics of many fusing systems. This range of diffuseness (0.75–1.5 fm) is quite larger than the usual value (0.66 fm) that has been used for the elastic scattering data. As a result, the standard WSP has systematically failed to give a simultaneous description of elastic scattering data and fusion data [28–34]. The concept of barrier distribution may be helpful in understanding the issues related to standard Woods-Saxon potential. The theoretical approach, wherein the barrier distribution is arising by the virtue of multidimensional aspect of the nucleus-nucleus potential, is very beneficial in this respect [35,36]. Siwek-Wilczynska and coworkers [37,38] have estimated the fusion cross sections and barrier distributions for different projectile-target combinations by using a theoretical technique based on the Gaussian function. Recently, Jiang *et al.* [39] have also analyzed the large set of experimental data by using the single Gaussian distribution function. Keeping this in view, the symmetric-asymmetric Gaussian barrier distribution (SAGBD) model has been introduced in the present work wherein the influences of dominant couplings have appeared as a cumulative effect. In the SAGBD approach, the Wong formula has been weighted by the Gaussian function and the nuclear structure effects are entering in model calculations via the multidimensional character of the nucleus-nucleus potential [40]. In addition, the present calculations have also estimated the quantitative reduction of the fusion barrier between reacting nuclei due to nuclear structure effects and hence have been analyzed in terms of the channel coupling parameter λ. Furthermore, attempts have been made to work out the percentage reduction of the effective fusion barrier with reference to the uncoupled Coulomb barrier and such effects have been described in terms of the parameter V_{CBRED}. The applicability of the present model has been tested for the fusion of $^{16}O + ^{70,72,73,74,76}Ge$ and $^{18}O + ^{74}Ge$ reactions.

As far as target isotopes are concerned, the series of $^{70,72,73,74,76}Ge$ isotopes is quite interesting and has displayed exciting features. It is due to the fact that with an increase in neutron richness, there are nuclear structural change effects [13,22]. In other words, as one moves from the ^{70}Ge to the ^{76}Ge nucleus, the Ge isotope gradually shifts from spherical symmetry to prolate deformed shape. In this sense, the type of dominant intrinsic channel which may be responsible for strong fusion enhancements at below barrier energies changes from vibrational couplings to rotational couplings. In the literature, the fusion data of the Ge isotope has been explored by using different projectiles within the framework of various models. Aguilera *et al.* [13] experimentally measured the precise fusion data of $^{16}O + ^{70,72,73,74,76}Ge$ reactions using a beam of ^{16}O from the tandem FN Van de Graaff accelerator at Notre Dame University on $^{70,72,73,74,76}Ge$ isotopes. The authors performed coupled channel calculations using the code CCDEF [34], wherein vibrational modes of colliding systems are coupled to their relative motion. In the theoretical analysis, authors [13] concluded that in the case of $^{16}O + ^{70,72,73}Ge$ reactions, vibrational degrees of freedom for a target are mandatory for the explanation of fusion enhancement at near and sub-barrier energies. The low-lying vibrational modes of ^{16}O lie at high excitation energies and hence are expected to have a very small influence on the fusion dynamics of chosen reactions. However, in the case of $^{16}O + ^{74,76}Ge$ reactions, the considerations of prolate deformations for both target nuclei are required in order to describe the fusion enhancement in the sub-barrier domain. Similar conclusions were made by authors in the analysis of $^{27}Al + ^{70,72,73,74,76}Ge$ [22] and $^{37}Cl + ^{70,72,73,74,76}Ge$ reactions [41]. Several studies [29,42–44] have emphasized that Ge isotopes were assumed to have fragile distortion and thus were extremely delicate nuclei. The experimental findings owing to Coulomb excitations [45], proton scattering [46], deuteron scattering [46], alpha-particle scattering [47], and electron scattering [48] have confirmed the spherical shape for $^{70,72,73}Ge$ isotopes and prolate deformed shapes for $^{74,76}Ge$ isotopes. Similar behaviors have been reported by other investigations based on the estimations of fusion cross sections [49,50].

From the other studies, Esbensen [51,52] and Zamrun *et al.* [53] have concluded that the ^{74}Ge nucleus has a spherical shape, and using coupled channel approach, the authors have reproduced the fusion data of ^{74}Ge with different projectiles like ^{27}Al, ^{64}Ni, and ^{74}Ge. Further, the authors have emphasized the influences of two phonon vibrational states of the ^{74}Ge nucleus on fusion of Ni + Ge and Ge + Ge systems. The proton scattering [54,55], deuteron scattering [56], and Li scattering [55] with $^{70,72}Ge$ isotopes have also indicated that there exist a two phonon $(0_2^+, 2_2^+, 4_1^+)$ structure for Ge nuclei. The fusion cross-section data for $^{18}O + ^{74}Ge$ and $^{16}O + ^{76}Ge$ reactions have been measured by Jia *et al.* [23]. The beams of $^{16,18}O$ from the HI-13 tandem accelerator of the China Institute of Atomic Energy (CIAE) Beijing, China in the energy range 38–61 MeV have been bombarded on ^{76}Ge and ^{74}Ge

targets, respectively. They have extracted the experimental data very precisely (within 8% of experimental uncertainties). The authors have considered the vibrational as well as rotational couplings for $^{16}O + ^{76}Ge$ reaction while only the vibrational coupling scheme has been used for the $^{18}O + ^{74}Ge$ reaction to explain the fusion dynamics at energies lying near and below the Coulomb barrier. For the $^{18}O + ^{74}Ge$ reaction, the additional coupling of PQNT (positive Q-value neutron transfer) channel has been found to add a small contribution to the fusion cross section at energies in the sub-barrier domain. However, in some cases like $^{40}Ca + ^{94,96}Zr$ or $^{28}Si + ^{94,96}Zr$ reactions, the PQNT channels strongly affect the sub-barrier fusion enhancement [57]. In this sense, the role of PQNT channel puzzles the sub-barrier fusion dynamics. Therefore, in addition to $^{16}O + ^{70,72,73,74,76}Ge$ reactions, the present work has also analyzed the fusion of the $^{18}O + ^{74}Ge$ reaction so that the possible effects of PQNT channels can be singled out from the vibrational couplings. In the present work, the theoretical calculations for the chosen reactions have been done by using the one-dimensional Wong formula, SAGBD model, and coupled channel approach [58]. For all the studied reactions, the calculated fusion cross sections and the extracted barrier distributions have matched approximately the experimental data. The similar behaviors of fusion cross sections and barrier distributions have been reflected from present coupled channel calculations. As has already been mentioned, the present calculations quantitively and qualitatively have estimated the channel coupling effects on the fusion process and these effects have been described in terms of channel coupling parameter λ and percentage reduction of the effective fusion barrier V_{CBRED}. As one moves from the $^{16}O + ^{70}Ge$ to the $^{16}O + ^{76}Ge$ reaction, the impacts of intrinsic degrees of freedom of collision partners become more peculiar and the same effects are reflected in the present model in terms of λ and V_{CBRED}. This directly reveals the shape transition effects for Ge isotopes. The maximum value of λ and V_{CBRED} for the $^{18}O + ^{74}Ge$ reaction have emphasized the additional contributions from the 2 n-transfer channel to the fusion process. The present coupled channel analysis which has been performed by using the coupled channel code CCFULL [58] has also suggested the importance of collective excitations and/or the neutron transfer channel in the fusion dynamics of chosen systems. Furthermore, attempts have been made to work out the contributions of entrance channel mass asymmetry on sub-barrier fusion cross sections of $^{16}O + ^{76}Ge$ and $^{18}O + ^{74}Ge$ reactions as both lead to the formation of the same compound nucleus (^{92}Zr) via different entrance channels. In the literature [59], it has been concluded that larger entrance channel mass asymmetry has enhanced fusion probability and has favored the fusion process. The entrance channel mass asymmetry has been larger for $^{16}O + ^{76}Ge$ in comparison to the $^{18}O + ^{74}Ge$ reaction. The 2 n-transfer channel with a positive Q value has been allowed for the $^{18}O + ^{74}Ge$ reaction while such channel has been suppressed in the case of the $^{16}O + ^{76}Ge$ reaction. Thus, SAGBD and the coupled channel method have pointed out that the sub-barrier fusion enhancement of the $^{18}O + ^{74}Ge$ reaction is larger than that of the $^{16}O + ^{76}Ge$ reaction at very low energy which has unambiguously confirmed the dominance of the PQNT channel over the entrance channel mass asymmetry effects.

We have formulated this paper as follows. In Sec. II, a brief description of the theoretical formalism, which is used in the present work, has been explained. The results and discussion for different systems under study are contained in Sec. III. Finally, the conclusions drawn are given in Sec. IV.

II. THEORETICAL FORMALISM

A. One-dimensional Wong formula

The total cross section for fusing nuclei in accordance to partial wave analysis is given by

$$\sigma_F = \frac{\pi}{k^2} \sum_{l=0}^{\infty} (2l+1)\, T_l^F \tag{1}$$

wherein T_l^F is the probability of transmission through the interaction barrier for the l^{th} partial wave and

$$k^2 = \frac{2\mu\, E_{c.m.}}{\hbar^2} \tag{2}$$

with reduced mass of fusing nuclei "μ" and incident energy in center of mass frame "$E_{c.m.}$." The probability of transmission for the Coulomb barrier can be calculated either by solving the Schrodinger wave equation or by using an approximate method [24,60]. Hill and Wheeler have proposed a simple expression for the transmission probability (T_l^{HW}) for the parabolic barrier and is defined as [25]

$$T_l^{HW} = \left[1 + \exp\left(\frac{2\pi}{\hbar\omega_l}(V_l - E_{c.m.})\right)\right]^{-1}, \tag{3}$$

where $\hbar\omega_l$ denotes the barrier curvature linked to the total fusion barrier (V_l) between colliding partners for the l^{th} partial wave. T_l^F in Eq. (1) can be replaced by T_l^{HW} and one obtains the following expression [40]:

$$\sigma_F = \frac{\pi}{k^2} \sum_{l=0}^{\infty} (2l+1)\, T_l^{HW}. \tag{4}$$

Using the following assumptions, Wong has further simplified the Hill-Wheeler approximation to obtain the analytical expression for fusion cross sections [40,61]:

$$R_l = R_{l=0} = R_B, \tag{5}$$

$$\omega_l = \omega_{l=0} = \omega_B, \tag{6}$$

$$V_l = V_{CB} + \frac{\hbar^2}{2\mu R_B^2}\left[l + \frac{1}{2}\right]^2, \tag{7}$$

where V_{CB} is the Coulomb barrier corresponding to $l = 0$, i.e., s wave. Using the above approximation and the integration of Eq. (4) from $l = 0$ to $l = \infty$, Wong has obtained the following formula for calculations of fusion cross sections around the Coulomb barrier:

$$\sigma^{Wong}(E_{c.m.}, V_{CB}) = \frac{\hbar\omega_B R_B^2}{2E_{c.m.}} \ln\left[1 + \exp\left(\frac{2\pi}{\hbar\omega_B}(E_{c.m.} - V_{CB})\right)\right], \tag{8}$$

wherein $\hbar\omega_B$, R_B, and V_{CB} are the barrier curvature, barrier position, and barrier height, respectively. Owing to the simplicity of the Wong formula, it is widely used to estimate the fusion cross sections for many fusing systems. In the present calculations, we adopt the Woods-Saxon form of nuclear potential and it is defined as

$$V_N(r) = -\frac{V_0}{\left[1+\exp\left(\frac{R-R_0}{a_0}\right)\right]}, \tag{9}$$

where V_0 is the depth and a_0 is the diffuseness of the nuclear potential. The radius parameter R_0 is related to the range r_0 via the following relation:

$$R_0 = r_0\left(A_P^{1/3} + A_T^{1/3}\right). \tag{10}$$

In the present work, we have attempted to work out the influences of channel coupling effects in terms of the parameter λ, which is extracted from the barrier distribution. If one chooses the deformed potential, then the magnitude of λ will be affected and in such a case, one can deduce the partial influences of the nuclear structure of colliding nuclei on the fusion process. However, for extracting out the impacts of nuclear structure associated with the participating nuclei unambiguously, we have considered the spherical Coulomb potential as well as the spherical nuclear potential. Therefore, the colliding nuclei are assumed to be spherical in shape and the corresponding Coulomb potential is defined as

$$V_C(r) = \frac{Z_P Z_T e^2}{r}, \tag{11}$$

where Z_P and Z_T denote the atomic number of projectile and target, respectively. The total interaction potential between the projectile and target system is defined as

$$V_l(r) = V_N(r) + V_C(r) + \frac{\hbar^2 l(l+1)}{2\mu r^2}. \tag{12}$$

For $l = 0$, the total interaction potential $V_l(r)$ is defined as

$$V_l(r)|_{l=0} = V(r) = V_N(r) + V_C(r), \tag{13}$$

$$V(r) = -\frac{V_0}{\left[1+\exp\left(\frac{R-R_0}{a_0}\right)\right]} + \frac{Z_P Z_T e^2}{r}. \tag{14}$$

Preferably, the height and peak position of the fusion barrier have been obtained by using following conditions at $r = R_B$:

$$\left.\frac{dV(r)}{dr}\right|_{r=R_B} = 0 \quad \text{and} \quad \left.\frac{d^2V(r)}{dr^2}\right|_{r=R_B} \leqslant 0, \tag{15}$$

where $V(r)$ denotes the total potential (i.e., nuclear + Coulomb). The height and barrier curvature of the Coulomb barrier respectively are evaluated by using the following relations:

$$V_{CB} = V(r)|_{r=R_B} \quad \text{and} \quad \hbar\omega_B = \left[-\frac{\hbar^2}{\mu}\left\{\frac{d^2V(r)}{dr^2}\right\}_{r=R_B}\right]^{1/2} \tag{16}$$

By employing the conditions given in Eqs. (15) and (16), we have obtained the values of barrier height, barrier position, and barrier curvature.

B. Symmetric-asymmetric Gaussian barrier distribution (SAGBD) model

In this section, we briefly define the theoretical formalism of the SAGBD model to calculate the fusion cross sections and related barrier distribution. The barrier distribution (BD) can be obtained by using the second order derivative of $E_{c.m.}\sigma^{Wong}$ with respect to $E_{c.m.}$. In Eq. (8), replacing V_{CB} by V_B, we get the following equation:

$$\sigma^{Wong}(E_{c.m.},\, V_B) = \frac{\hbar\omega_B R_B^2}{2E_{c.m.}} \ln\left[1+\exp\left(\frac{2\pi}{\hbar\omega_B}(E_{c.m.}-V_B)\right)\right], \tag{17}$$

or

$$E_{c.m.}\sigma^{Wong} = \frac{\hbar\omega_B R_B^2}{2} \ln\left[1+\exp\left(\frac{2\pi}{\hbar\omega_B}(E_{c.m.}-V_B)\right)\right]. \tag{18}$$

Differentiating Eq. (18) with respect to $E_{c.m.}$,

$$\frac{d}{dE_{c.m.}}(E_{c.m.}\sigma^{Wong}) = \pi R_B^2\left[\frac{1}{1+\exp\left(\frac{2\pi}{\hbar\omega_B}(E_{c.m.}-V_B)\right)}\right]\exp\left(\frac{2\pi}{\hbar\omega_B}(E_{c.m.}-V_B)\right).$$

The second order derivative of $E_{c.m.}\sigma^{Wong}$ with $E_{c.m.}$ is known as the barrier distribution (BD) and can be written as

$$BD = \frac{d^2}{dE_{c.m.}^2}(E_{c.m.}\sigma^{Wong}) = \pi R_B^2\frac{d}{dE_{c.m.}}\left[\frac{\exp\left(\frac{2\pi}{\hbar\omega_B}(E_{c.m.}-V_B)\right)}{1+\exp\left(\frac{2\pi}{\hbar\omega_B}(E_{c.m.}-V_B)\right)}\right],$$

$$BD = \pi R_B^2\frac{d}{dE_{c.m.}}\left[\frac{1}{1+\exp\left(-\frac{2\pi}{\hbar\omega_B}(E_{c.m.}-V_B)\right)}\right] = \pi R_B^2\frac{dT}{dE_{c.m.}},$$

where T is the tunneling probability for the fusion barrier. The tunneling probability (T) is defined as

$$T = \frac{1}{\left[1+\exp\left(-\frac{2\pi}{\hbar\omega_B}(E_{c.m.}-V_B)\right)\right]}. \tag{19}$$

By rearranging the term, we get

$$BD = \pi R_B^2 \frac{\exp\left(-\frac{2\pi}{\hbar\omega_B}(E_{c.m.} - V_B)\right)}{\left[1 + \exp\left(-\frac{2\pi}{\hbar\omega_B}(E_{c.m.} - V_B)\right)\right]^2} \frac{2\pi}{\hbar\omega_B}. \quad (20)$$

Let

$$x = \frac{2\pi}{\hbar\omega_B}(E_{c.m.} - V_B). \quad (21)$$

Using Eq. (21) in Eq. (20), the effective barrier distribution $D_f(V_B)$ can be written as

$$D_f = \frac{BD}{\pi R_B^2} = \frac{1}{\pi R_B^2}\frac{d^2}{dE_{c.m.}^2}(E_{c.m.}\,\sigma^{Wong}) = \frac{2\pi}{\hbar\omega_B}\frac{e^{-x}}{[1+e^{-x}]^2},$$

$$D_f = \frac{2\pi}{\hbar\omega_B}\frac{e^{x}}{[1+e^{x}]^2} = \delta(E_{c.m.} - V_B). \quad (22)$$

Equation (20) or Eq. (22) shows a single peak, which is symmetric around $E_{c.m.} = V_B$. The width of this peak is narrow and depends upon barrier curvature via relation $\hbar\omega_B \ln(3+\sqrt{8})/\pi = 0.56\hbar\omega_B$ [15,19]. The behavior of Eq. (20) or Eq. (22) is smooth due to the quantum tunneling phenomenon and various kinds of channel coupling effects that are actively involved in the fusion process. Therefore, the realistic barrier under consideration includes the nuclear structure effects and hence it is of multidimensional character. Following Stelson's model [15], the shape of the barrier distribution can be approximately recovered for many projectile-target combinations if one considers the Gaussian type of weight function. The effective barrier distribution $D_f(V_B)$ obeys the following normalization condition:

$$\int D_f(V_B)\, dV_B = 1. \quad (23)$$

In order to take into account the multidimensional character of the realistic barrier, the total fusion cross section is obtained by weight average of the one-dimensional Wong formula. The weighted fusion cross section is defined as

$$\sigma_F = \int_0^\infty D_f(V_B)\,\sigma^{Wong}(E_{c.m.}, V_B)\, dV_B, \quad (24)$$

wherein $\sigma^{Wong}(E_{c.m.}, V_B)$ is the Wong formula as defined in Eq. (17). $D_f(V_B)$ can be taken as a continuous and symmetric function like distributions of a Gaussian type function. In general, the shape of the real barrier distribution is found to be asymmetric with respect to the average barrier height in the barrier distribution. Therefore, the asymmetric Gaussian function can be used for the real barrier distribution. However, in the present work, we test a symmetric Gaussian function to recover the shape of the realistic barrier distribution. The symmetric Gaussian function is defined as

$$D_f(V_B) = \frac{1}{N}\exp\left[-\frac{(V_B - V_{B0})^2}{2\Delta^2}\right] \quad (25)$$

with $N = \Delta\sqrt{2\pi}$.

Δ in this equation is the standard deviation and corresponds to the half width of the peak or barrier distribution $D_f(V_B)$ at about 60% of the full width. The mean barrier height V_{B0} can be quantitatively described in terms of the effective barrier height $V_{\rm eff}$ and approximately lies within the range

$$V_{B0} \approx (0.994 \pm 0.003)\, V_{\rm eff}. \quad (26)$$

The effective barrier height $V_{\rm eff}$ extracted from the barrier distribution equals the peak position of the barrier distribution. Due to the involvement of various channel coupling effects, the value of $V_{\rm eff}$ was found to be less than that of the Coulomb barrier V_{CB}. Here, $V_{\rm eff}$ lies within the range as given below:

$$V_{\rm eff} \approx (0.95 \pm 0.03)\, V_{CB}. \quad (27)$$

Full width at half maximum (FWHM) is defined as the full width of peak or barrier distribution $D_f(V_B)$ at about 50% of the full width,

$$2\text{FWHM} = 2\Delta\sqrt{2\ln 2} = 2.355\Delta. \quad (28)$$

In the present work, we extract the quantitative contribution of channel couplings which arise due to the nuclear structure of the participant. Such contribution is described in terms of λ which is defined below:

$$\lambda = V_{CB} - V_{\rm eff}, \quad (29)$$

where V_{CB} is the Coulomb barrier.

III. RESULTS AND DISCUSSION

A. Sensitivity of fusion data towards potential parameters

Figure 1 shows the comparison of the Coulomb barriers for the fusing reactions under study. From this figure, one can easily notice that the heights of the Coulomb barriers are different for different reactions. In other words, the radial dependence of interaction barriers near the peak is different causing the different barrier characteristics for chosen systems. As a result, the magnitude of sub-barrier fusion enhancements depends upon the projectile-target combination. In the present work, we take Woods-Saxon parametrization

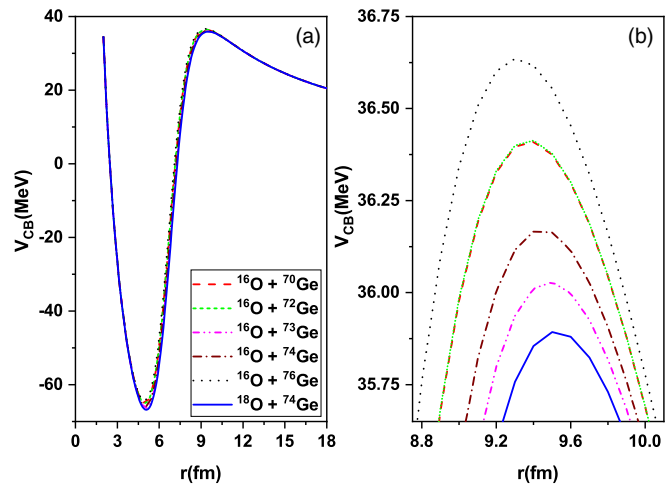

FIG. 1. (a) The variation of the Coulomb barrier (V_{CB}) as a function of radial separation between projectile and target for the ^{16}O + ^{70,72,73,74,76}Ge and ^{18}O + ^{74}Ge reactions, and (b) amplified version of (a) near barrier positions.

TABLE I. The parameters of the Woods-Saxon potential such as depth (V_0), diffuseness (a_0), and range (r_0), which have been used to analyze the experimental data for different heavy ion fusing systems.

Colliding systems	V_0 (MeV)	a_0 (fm)	r_0 (fm)
$^{16}O+^{70}Ge$	150	0.68	1.015
$^{16}O+^{72}Ge$	150	0.68	1.004
$^{16}O+^{73}Ge$	150	0.68	1.015
$^{16}O+^{74}Ge$	150	0.68	1.008
$^{16}O+^{76}Ge$	150	0.68	0.985
$^{18}O+^{74}Ge$	150	0.68	1.002

of nuclear potential wherein depth, range, and diffuseness parameters have been extracted by reproducing the above barrier fusion data of studied reactions. The sub-barrier fusion data points have strong dependence upon the nuclear structure effects of the participating nuclei, whereas the above barrier fusion data points are quite insensitive towards channel coupling effects. Therefore, the above barrier fusion data should be reproduced by the one-dimensional barrier penetration model. For extracting the potential parameters, the depth (V_0) is kept fixed at 150 MeV while the range (r_0) and diffuseness parameter (a_0) are varied in order to reproduce the fusion data around the Coulomb barrier. In this way, we also investigate the sensitivity of fusion cross-section data and experimental barrier distribution with respect to change in potential parameters and the details of the results are shown in Figs. 3 and 4. The values of potential parameters that recover the fusion cross-section and experimental barrier distribution are listed in Table I. By choosing the potential parameters as listed in Table I, we obtain the Coulomb barrier (V_{CB}), the position of the peak of the Coulomb barrier (R_B), and the barrier curvature ($\hbar\omega_B$) by employing the conditions defined through Eqs. (14)–(16). The so obtained barrier characteristics are listed in Table II and are used in the present calculations.

In Fig. 2, the radial dependence of the standard WSP, Coulomb potential, and total interaction potential (Coulomb barrier) for different reactions is depicted. In this figure, the solid line in each panel shows the Coulomb barrier. The nuclear potential (V_N) is attractive, while the Coulomb potential (V_C) is repulsive in nature and a combination of these forms the Coulomb barrier (V_{CB}). The dash line in each panel denotes the radial dependence of Coulomb potential, while dash dot-dot line in each panel denotes the radial dependence of the nuclear potential.

TABLE II. The values of Coulomb barrier height (V_{CB}), barrier position (R_B), and barrier curvature ($\hbar\omega_B$) obtained by using Eqs. (14)–(16) for different heavy ion fusing systems.

Colliding systems	V_{CB} (MeV)	R_B (fm)	$\hbar\omega_B$ (MeV)
$^{16}O+^{70}Ge$	36.36	9.50	2.64
$^{16}O+^{72}Ge$	36.38	9.50	2.63
$^{16}O+^{73}Ge$	36.02	9.50	3.02
$^{16}O+^{74}Ge$	36.16	9.50	2.86
$^{16}O+^{76}Ge$	36.62	9.25	3.45
$^{18}O+^{74}Ge$	35.89	9.50	3.01

To investigate the dependence of fusion cross section and related barrier distribution on the choice of potential parameters, the theoretical results are shown in Figs. 3 and 4. In Fig. 3, keeping potential depth (V_0) and diffuseness (a_0) fixed at 150 MeV and 0.68 fm respectively, the fusion cross section and barrier distribution are obtained by varying the range parameter (r_0). For the given value of V_0 and a_0, the magnitude of the fusion cross section increases with an increase of the range parameter, which indicates that the effective fusion barrier between the fusing pairs decreases with an increase in the range parameter. For $r_0 = 1.025$ fm, the theoretical outcomes of fusion cross sections overestimate the experimental data at below barrier energies while at above barrier energies, the calculated results approximately reproduce the fusion data as shown in Fig. 3(a). The same calculations do not fit the experimental barrier distribution in the entire range of energies as shown in Fig. 3(b). This indicates that the dominant channel coupling effects that are responsible for sub-barrier fusion enhancement are not recovered reasonably by such calculations. For $r_0 = 0.995$ fm, the theoretical cross sections obtained by SAGBD calculations underestimate the fusion data in the entire range of incident energies and similar conclusions are also reflected from the corresponding barrier distribution. For $r_0 = 1.015$ fm, the fusion cross sections and the corresponding barrier distribution predicted by the present calculations approximately recover the experimental data in near and above barrier regions. This suggests that the various channel coupling effects that lead to significantly larger sub-barrier fusion cross sections with respect to expectations of 1-DBPM are now properly addressed by the SAGBD calculations.

In order to strengthen the above conclusions, the dependence of the fusion cross section and barrier distribution on the diffuseness parameter of the Woods-Saxon potential is also investigated and the results are shown in Fig. 4. As the diffuseness parameter increases, the height of fusion barrier decreases and the corresponding fusion cross section increases with reference to the outcomes of 1-DBPM. In this figure, the potential depth (V_0) and range (r_0) are kept fixed at 150 MeV and 1.015 fm respectively while the values of the diffuseness parameter (a_0) are varied. For $a_0 = 0.63$ fm, the calculated fusion cross section underestimates the fusion data in the entire range of incident energies [see Fig. 4(a)]. Similar results are reflected from barrier distribution calculations as shown in Fig. 4(b), wherein the barrier distributions obtained for $a_0 = 0.63$ fm do not match the experimental data. For $a_0 = 0.71$ fm, the calculated fusion cross sections and barrier distributions overestimate the experimental data in sub-barrier energy regions, while at above barrier energies the fusion cross-section data are reasonably reproduced. Similar conclusions are also inferred from the barrier distribution. For $a_0 = 0.68$ fm, the calculated fusion cross section and the corresponding barrier distribution appropriately address the experimental data and hence reasonably recover the effects of the nuclear structure of participating nuclei. The calculated results shown in Figs. 3 and 4 unambiguously indicate that the outcomes of the model are quite sensitive to the choice of potential parameters used for the predictions of the fusion

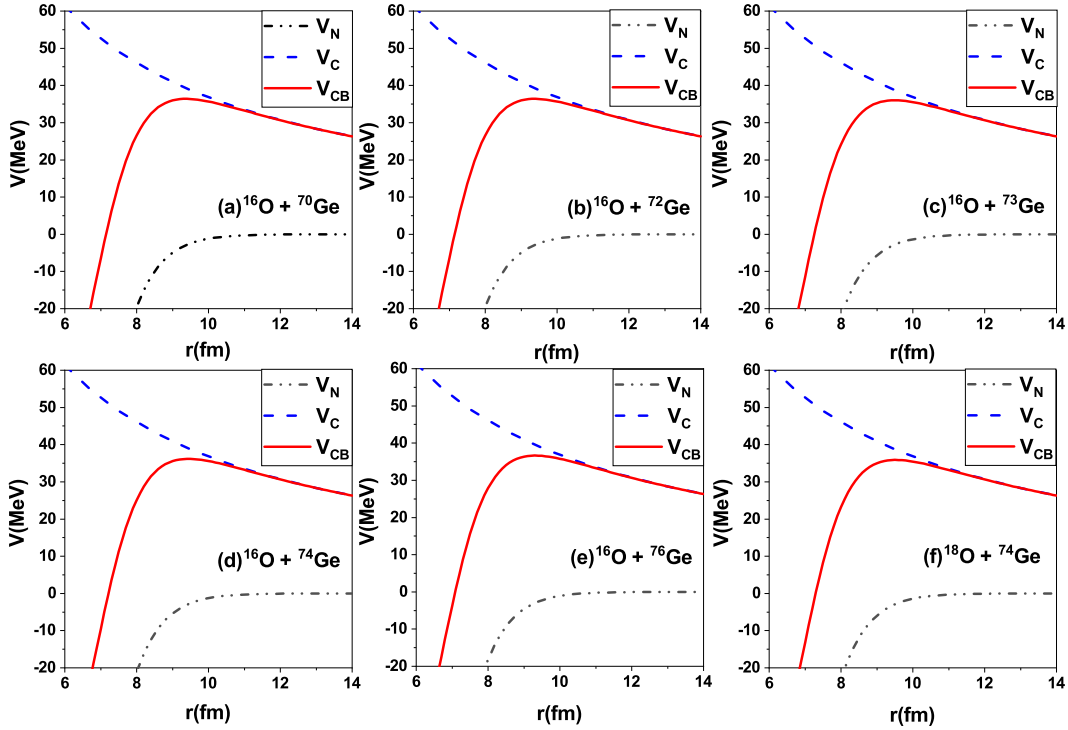

FIG. 2. The variations of the Coulomb (V_C) and nuclear (V_N) potentials along with the Coulomb barrier (V_{CB}) as a function of radial separation between projectile and target for (a) ^{16}O + ^{70}Ge, (b) ^{16}O + ^{72}Ge, (c) ^{16}O + ^{73}Ge, (d) ^{16}O + ^{74}Ge, (e) ^{16}O + ^{76}Ge, and (f) ^{18}O + ^{74}Ge systems.

cross sections and related physical quantities. The behaviors of the fusion cross section and barrier distribution are similar for all studied reactions.

B. Wong model and SAGBD model analysis of fusion data

In Figs. 5(a) and 5(b), the fusion cross sections calculated by using Wong and the SAGBD model are shown for the ^{16}O + ^{70}Ge and ^{16}O + ^{72}Ge reactions, respectively. In each figure, the solid line denotes the calculations obtained by using the SAGBD model and the dash line refers to Wong calculations, while symbols denote the experimental data. As the one-dimensional Wong formula does not consider the influence of channel coupling effects that arise due to the nuclear structure of the participating nuclei, the calculated fusion cross sections are strongly underpredicted with respect to

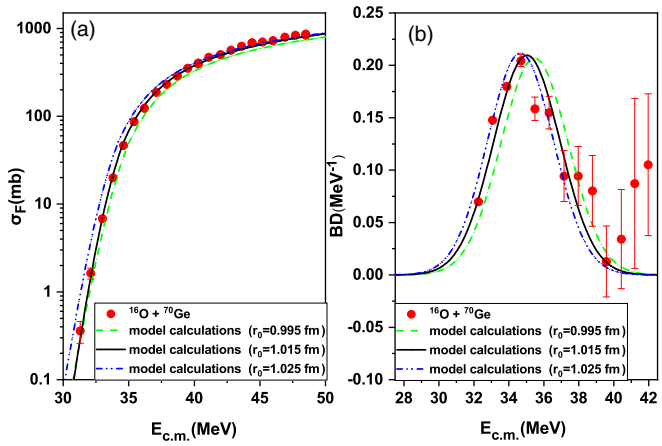

FIG. 3. The fusion cross section (a) and barrier distribution (b) for ^{16}O + ^{70}Ge reaction as a function of energy in center-of-mass frame "$E_{c.m.}$" for different values of range (r_0) parameter. The fusion cross section and barrier distribution obtained by using the SAGBD model are compared with experimental data taken from Ref. [13].

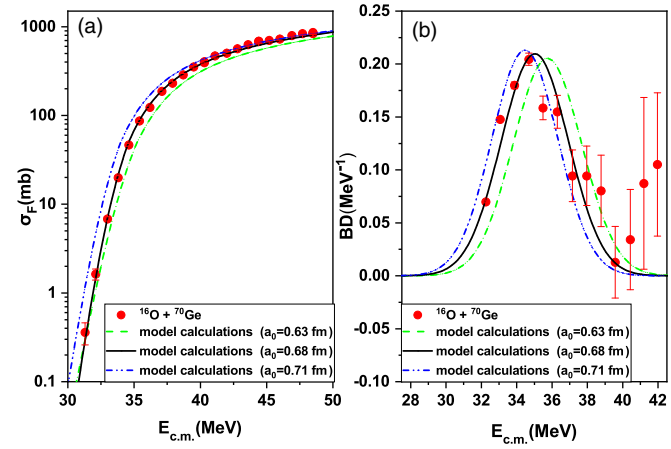

FIG. 4. The fusion cross section (a) and barrier distribution (b) for ^{16}O + ^{70}Ge reaction as a function $E_{c.m.}$ for different values of diffuseness (a_0) parameter. The fusion cross section and barrier distribution obtained by using the SAGBD model are compared with the experimental data taken from Ref. [13].

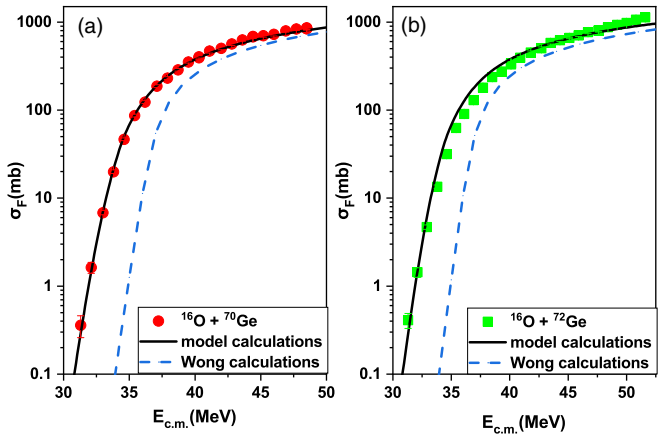

FIG. 5. The fusion cross section of $^{16}O + ^{70}Ge$ (a) and $^{16}O + ^{72}Ge$ (b) reactions as a function of $E_{c.m.}$ obtained by using Wong formula and SAGBD model. These results are compared with the experimental data taken from Ref. [13].

experimental data in the entire energy range. These calculations are performed by taking the parameters of the fusing systems as listed in Table I. Since there are no barrier modulation effects in the simple Wong formula, the shape of the barrier distribution cannot be recovered by using such outcomes. That is why the predictions of the one-dimensional Wong formula remain sufficiently smaller than that of the fusion data in the entire energy range. This clearly suggests that channel coupling effects which are induced due to the nuclear structure of fusing nuclei are extremely important in the sub-barrier domain and without considering them one cannot reproduce the fusion data at near and sub-barrier energies. Similar behaviors of fusion cross sections based on the Wong formula have been found for all the studied reactions (see Figs. 5, 7, and 9).

Aguilera *et al.* [13] reported that the fusion cross-section data of $^{16}O + ^{70,72}Ge$ reactions are enhanced with reference to the predictions made by the 1-DBPM. The cause of such enhancements is found to have a link with the vibrational degrees of freedom associated with both collision partners. Without the inclusion of low-lying states like 2^+ and 3^- vibrational states of the target and 2^+ state of the projectile, one cannot achieve a good description of fusion data of chosen reactions. Gautam and co-workers [16,26,50], using CCFULL and EDWSP model calculations, also arrived at similar conclusions and emphasized that vibrational couplings for the target play a very crucial role in the enhancement of fusion cross sections at sub-barrier energies. In the present case due to the inclusion of multidimensional character, the model calculations automatically entertain the dominant channel coupling effects in sub-barrier fusion dynamics of given reaction. In other words, the multidimensional character of the nucleus-nucleus potential that arises due to nuclear structure effects is intrinsically smeared in the SAGBD calculations. This reduces the fusion barrier between fusing partners and consequently predicts larger fusion cross sections at sub-barrier energies. In this sense, the model calculations shift towards the experimental data in below barrier energy regions and hence reasonably explain the observed sub-barrier fusion enhancements with respect to the outcomes of 1-DBPM.

If there is no channel coupling effects then the peak of the barrier distribution occurs around the Coulomb barrier. However, due to the inclusion of intrinsic degrees of freedom, the height as well as the shape of the main peak of barrier distribution changes and may be shifted to the left or right side of the Coulomb barrier and such effects in the present model are represented in terms of the channel coupling parameter λ. Therefore, λ intrinsically relates to the various kinds of nuclear structure effects that are responsible for sub-barrier fusion enhancement. In the present model, the position of the main peak of barrier distribution represents the effective barrier height $V_{\rm eff}$ between fusing nuclei and is approximately defined by Eq. (27). The left shift of main peak of the barrier distribution with reference to the uncoupled Coulomb barrier V_{CB} represents the reduction of the fusion barrier, and the right shift of the main peak represents the increase of the fusion barrier with reference to the uncoupled Coulomb barrier. The FWHM of the effective barrier distribution is defined by Eq. (28). The parameter V_{CBRED} represents the percentage deviation or reduction of the effective fusion barrier between colliding nuclei with respect to the uncoupled Coulomb barrier V_{CB} due to the consideration of various nuclear structure effects associated with reacting nuclei. $R_{\rm eff}$ is the peak position of the effective fusion barrier ($V_{\rm eff}$) between the fusion partners. The various parameters of the effective barrier distribution, which are extracted from the SAGBD model calculations, are listed in Table III.

For $^{16}O + ^{70,72}Ge$ reactions, the barrier distributions obtained from the SAGBD model are compared with the experimental barrier distribution obtained by using the three-point difference method and the results are shown in Fig. 6. As the shape and height of the barrier distribution are quite sensitive to the nature of the dominant channel coupling effects, the shape of barrier distribution can only be recovered if one includes the nuclear structure effects of the fusing nuclei. If theoretical calculations do not consider the nuclear structure effects like vibrational degrees of freedom of the target for $^{16}O + ^{70,72}Ge$ reactions, then the shape of the barrier distribution cannot be reproduced. The coupled channel analysis due to Aguilera *et al.* [13] pointed out the significance of the low-lying vibrational state of $^{70,72}Ge$ nuclei in the sub-barrier fusion enhancement of chosen systems. The inclusion of vibrational degrees of freedom for colliding nuclei like 2^+ and 3^- quantum states in the target reproduce the magnitude of sub-barrier fusion enhancement and the shape of barrier distribution. As the vibrational states of projectile (^{16}O) lie at high excitation energies, such quantum states are not expected to affect the barrier distribution. In the present work, the shape of barrier distribution for $^{16}O + ^{70,72}Ge$ reactions can be reasonably reproduced by considering the symmetric Gaussian function. The channel coupling parameter (λ) has been found to have a value $\lambda = 1.32$ and $\lambda = 1.33$ for $^{16}O + ^{70}Ge$ and $^{16}O + ^{72}Ge$ reaction, respectively. The parameter V_{CBRED} intimates that the effective fusion barrier between fusing partners decreases due to nuclear structure effects of reacting nuclei by 3.64% of V_{CB} for $^{16}O + ^{70}Ge$ and 3.66% of V_{CB} for $^{16}O + ^{72}Ge$ reaction (see Table III).

TABLE III. The parameters like standard deviation Δ , mean barrier height V_{B0} and effective barrier height $V_{\rm eff}$, Coulomb barrier (V_{CB}), the channel coupling parameter λ, FWHM, V_{CBRED}, $R_{\rm eff}$ for different systems are listed.

Colliding systems	Δ (MeV)	V_{B0} (MeV)	$V_{\rm eff}$ (MeV)	V_{CB} (MeV)	$\lambda = (V_{CB} - V_{\rm eff})$ (MeV)	FWHM (MeV)	V_{CBRED} (MeV)	$R_{\rm eff}$ (fm)
$^{16}O + ^{70}Ge$	1.90	34.80	35.04	36.36	1.32	4.47	3.64% of V_{CB}	10.52
$^{16}O + ^{72}Ge$	1.91	34.81	35.05	36.38	1.33	4.49	3.66% of V_{CB}	10.51
$^{16}O + ^{73}Ge$	1.88	34.47	34.69	36.03	1.34	4.42	3.72% of V_{CB}	10.62
$^{16}O + ^{74}Ge$	1.89	34.61	34.80	36.16	1.36	4.45	3.77% of V_{CB}	10.59
$^{16}O + ^{76}Ge$	1.92	35.05	35.24	36.62	1.38	4.52	3.78% of V_{CB}	10.46
$^{18}O + ^{74}Ge$	1.88	34.34	34.50	35.89	1.39	4.42	3.88% of V_{CB}	10.68

The fusion cross sections for $^{16}O + ^{73,74}Ge$ reactions are estimated by using the Wong formula as well as the SAGBD model and the results are shown in Fig. 7. For the $^{16}O + ^{73}Ge$ reaction, Aguilera *et al.* [13] suggested that the ^{73}Ge isotope lies in the transition phase between the spherical and prolate deformed shapes. Due to the odd-*A* nature, the ^{73}Ge isotope exhibits a large number of low-lying quantum states and their involvement increases the fusion probability, and thus the resulting fusion cross sections are found to be much larger than that of $^{16}O + ^{70,72}Ge$ reactions. Using the coupled channel approach, the authors successfully explained the influences of odd-*A* quantum states of a target on fusion dynamics of the $^{16}O + ^{73}Ge$ reaction. The authors also pointed out that only intrinsic degrees of freedom of a target are not enough to reproduce the fusion data in the entire range of incident energies. Hence, the couplings to projectile excitations are necessarily needed to account for the sub-barrier fusion enhancement of the chosen system. However, the SAGBD calculations consider the channel coupling effects via barrier distribution and henceforth intrinsically include their impacts in the heavy-ion fusion dynamics. As a result, the model calculations predict the larger fusion cross sections with reference to outcomes of the Wong formula and consequently reproduce the experimental data around the Coulomb barrier, while the calculations based on the Wong formula strongly underestimate the fusion data in near and above barrier energy regions. This signifies the importance of nuclear structure effects on the fusion dynamics of the $^{16}O + ^{73}Ge$ reaction.

The fusion dynamics of the $^{16}O + ^{74}Ge$ reaction is quite interesting due to the fact that the ^{74}Ge isotope is expected to have a statically deformed shape (prolate deformed shape) in its ground state. Aguilera *et al.* [13] pointed out that rotational states of a target significantly affect the sub-barrier fusion dynamics of the $^{16}O + ^{74}Ge$ reaction and hence by considering the aforementioned states, authors reproduced the sub-barrier fusion enhancement and the shape of barrier distribution. This prolate deformed character of a target isotope has been experimentally supported by the measurements based on Coulomb excitations [45] and the electron scattering method [48]. In contrast, Zamrun *et al.* [53] and Esbensen [51,52], based on the more refined coupled channel analysis, concluded that the ^{74}Ge isotope has a vibrational rather than statically deformed shape and thus recovered the fusion cross-section data and barrier distribution for $^{64}O + ^{74}Ge$, $^{74}Ge + ^{74}Ge$, $^{16}O + ^{74,76}Ge$, and $^{27}Al + ^{74,76}Ge$ reactions. For the $^{16}O + ^{74}Ge$ reaction, the theoretical results that we obtain by using the one-dimensional Wong formula are substantially smaller at sub-barrier energies while such calculations closely match the experimental data at above barrier energies. The outcomes based on the SAGBD model intrinsically incorporate the various channel coupling effects and thus

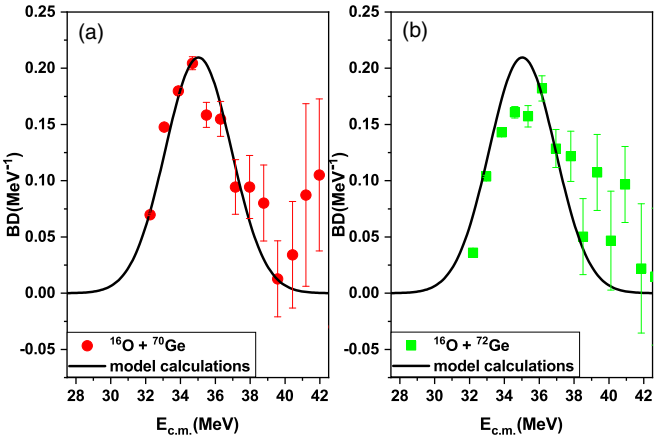

FIG. 6. The barrier distribution (BD) for $^{16}O + ^{70}Ge$ (a), and $^{16}O + ^{72}Ge$ reactions as a function of $E_{c.m.}$. The discrete symbols denote the barrier distribution data [13] obtained by using double differentiation method [17]. For both cases, the solid line denotes the outcomes of the present model.

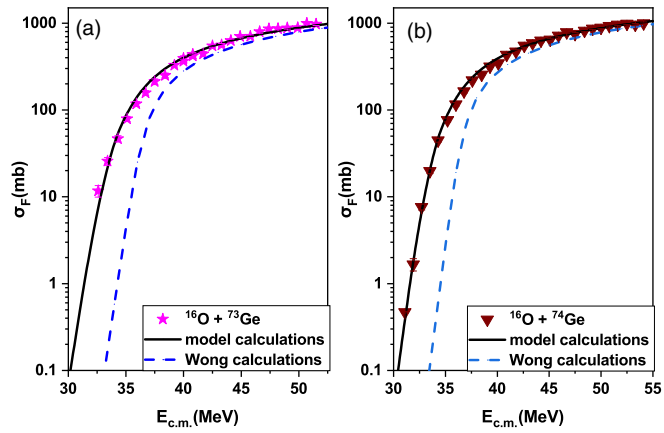

FIG. 7. Same as Fig. 5 but for $^{16}O + ^{73}Ge$ (a) and $^{16}O + ^{74}Ge$ (b) reactions. The results are compared with experimental data taken from Ref. [13].

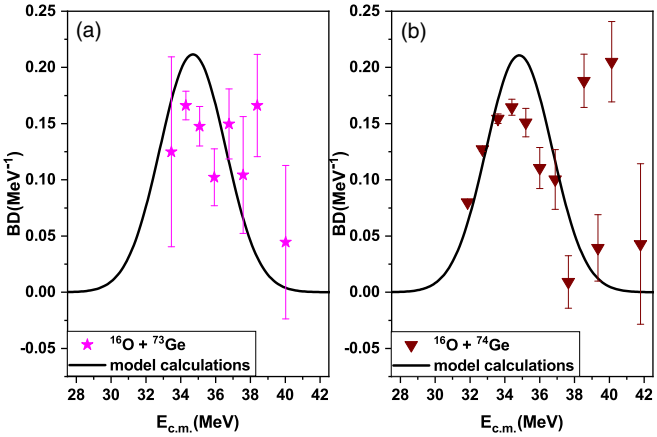

FIG. 8. Same as in Fig. 6 but for $^{16}O + ^{73}Ge$ (a) and $^{16}O + ^{74}Ge$ (b) reactions.

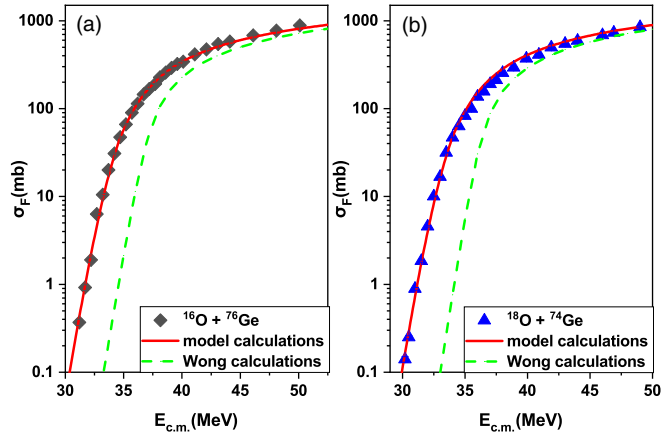

FIG. 9. Same as Fig. 5 but for $^{16}O + ^{76}Ge$ (a) and $^{18}O + ^{74}Ge$ (b) reactions. The results are compared with experimental data taken from Ref. [23].

appropriately address the fusion data in close vicinity of the Coulomb barrier for a system under consideration.

The barrier distributions of $^{16}O + ^{73,74}Ge$ reactions, which are obtained by using the SAGBD model, are compared with the experimental barrier distribution and results are shown in Fig. 8. The SAGBD results and experimental barrier distributions are in close agreement with each other. As pointed out in the literature, the large number of odd-A quantum states for the ^{73}Ge isotope, which are included in the coupled channel analysis, significantly modify the fusion probability as well as sub-barrier fusion cross sections. Therefore, the coupled channel calculations due to Aguilera *et al.* [13] adequately address the fusion data. On the other hand, the present model includes the cumulative effects of nuclear structure of reaction partners and hence recovers the shape of experimental barrier distribution of $^{16}O + ^{73}Ge$ reaction. Aguilera *et al.* [13] suggested that the ^{74}Ge nucleus has a prolate deformed shape in its ground state and the considerations of static deformation of target enhance the magnitude of fusion cross sections and hence reasonably reproduce the shape of experimental barrier distribution. However, studies based on more advanced coupled channel analysis indicated that ^{74}Ge has a spherical shape. Since the present model calculations recover the behavior of the fusion cross sections and experimental barrier distribution, model outcomes partially or fully include the effects of the nuclear structure of fusing pairs. The channel coupling parameters λ and V_{CBRED} for $^{16}O + ^{73,74}Ge$ reactions are listed in Table III, which indicates that there is a reduction of fusion barrier due to the inclusion of projectile as well as target degrees of freedom. The channel coupling parameter is found to have the values $\lambda = 1.34$ and $\lambda = 1.36$ for the $^{16}O + ^{73}Ge$ and $^{16}O + ^{74}Ge$ reactions, respectively. The values of V_{CBRED} indicate that the effective fusion barrier between collision partners decreases by 3.72% of V_{CB} for $^{16}O + ^{73}Ge$ and 3.77% of V_{CB} for the $^{16}O + ^{74}Ge$ reaction.

Jia *et al.* [23] experimentally measured the fusion cross-section data for $^{18}O + ^{74}Ge$ and $^{16}O + ^{76}Ge$ reactions. For the $^{16}O + ^{76}Ge$ reaction, the projectile is assumed to be spherical in its ground state while the target is expected to have a prolate deformed shape. Aguilera *et al.* [13] used the statically deformed shape and β_2 and β_4 deformation for the ^{76}Ge-nucleus which reasonably reproduced the magnitude of the fusion cross section as well as the barrier distribution. Jia *et al.* [23] used the coupled channel analysis and arrived at similar conclusions. The sub-barrier fusion enhancement of this reaction with respect to 1-DBPM can only be linked with the statically deformed shape of the target isotope. Similar conclusions were drawn by Gautam *et al.* [26] based on EDWSP and coupled channel predictions. In the present case, the predictions that are made by the Wong calculations remain sufficiently smaller than that of the experimental data particularly at below barrier energies as shown in Fig. 9. However, the predictions based on the SAGBD model adequately address the experimental data in the entire range of energies spreading around the Coulomb barrier. This points toward the multidimensional character of the present model, which includes the impacts of static deformation associated with target isotope in theoretical outcomes.

Jia *et al.* [23] considered vibrational couplings for the ^{74}Ge isotope and reproduced the experimental data of the $^{18}O + ^{74}Ge$ reaction and, in turn, concluded that ^{74}Ge has vibrational character. *Gautam et al.* [26], used the coupled channel and EDWSP based calculations and intimated that ^{74}Ge has a spherical shape while ^{76}Ge has a prolate deformed shape in its ground state. Dobaczewski *et al.* [62] ^{76}Ge used Skyrme Hartree-Fock theory and pointed out that the ^{74}Ge nucleus is spherical in its ground state. This conclusion was further supported by Sharma *et al.* [63] by using the relativistic mean field theory for predicting spherical shape of ^{74}Ge isotope. The projectile ^{18}O is also spherical in its ground state and the low-lying vibrational states of ^{18}O lie at lower excitation energies than that of the ^{16}O isotope. Therefore, the ^{18}O nucleus is expected to be actively involved in the fusion process. This unambiguously revealed that the vibrational excitations of both collision partners for $^{18}O + ^{74}Ge$ are the dominant mode of couplings. Additionally, the fusion of the $^{18}O + ^{74}Ge$ reaction offers a $2n$ channel with positive Q value and involvement of such a channel strongly affects fusion cross sections at near and sub-barrier energies. Jia *et al.* [23] considered the

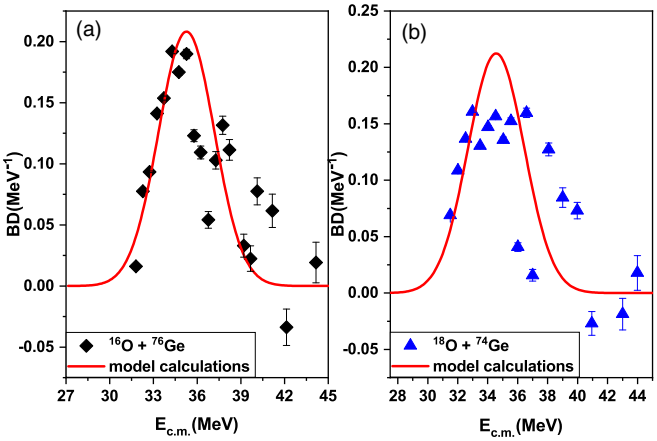

FIG. 10. Same as Fig. 6 but for the $^{16}O + ^{76}Ge$ (a) and $^{18}O + ^{74}Ge$ (b) reactions. The results are compared with the experimental data taken from Ref. [23].

2 *n*-pickup channel along with the vibrational couplings of the projectile and target, and henceforth adequately recovered the experimental data of the $^{18}O + ^{74}Ge$ reaction. The fusion cross sections that are obtained by using the simple Wong formula and the SAGBD model for the $^{18}O + ^{74}Ge$ reaction are shown in Fig. 9(b). The calculations based on the Wong formula are appreciably smaller than the fusion data in the near and sub-barrier energy regions. On the other hand, the close agreement between experimental data and the SAGBD model predictions clearly reflects that the influences of the neutron transfer channel with positive Q value are intrinsically included in the present calculations.

In Fig. 10, the extracted barrier distributions for the $^{16}O + ^{76}Ge$ and $^{18}O + ^{74}Ge$ reactions are compared with the experimental data. The experimental barrier distribution for $^{16}O + ^{76}Ge$ has been adequately reproduced by the model calculations, while for the $^{18}O + ^{74}Ge$ reaction the model calculations approximately recover the shape of experimental barrier distribution. For the $^{16}O + ^{76}Ge$ reaction, the dominant effects of static deformation and higher order deformation for a target appear in the experimental as well as the predicted barrier distribution. The coupled channel analysis of Aguilera *et al.* [13] and Jia *et al.* [23] adequately addressed the experimental distribution of $^{16}O + ^{76}Ge$ reaction by considering the deformed shape of the target nucleus ^{76}Ge. Similarly, the SAGBD calculations reproduce the experimental data of the $^{16}O + ^{76}Ge$ reaction and hence analogous conclusions as inferred from the pioneering work of Aguilera *et al.* [13] and Jia *et al.* [23] are also reflected in the present work. In the case of the $^{18}O + ^{74}Ge$ reaction, there exists a pair of neutron transfer channels with a positive Q value and the shape of the barrier distribution is expected to be broadened with respect to that of other systems. Although the height of the experimental barrier distribution of the $^{18}O + ^{74}Ge$ reaction is slightly smaller than that of the other fusing partners, broadening effects in the barrier distribution are weak. This broadening of the barrier distribution may arise as a result of the formation of the neck region due to neutron transfer between collision partners in the entrance channel. The present model calculations appropriately recover the shape of the experimental barrier distribution for the $^{18}O + ^{74}Ge$ reaction. The channel coupling parameter is found to have the values $\lambda = 1.38$ and $\lambda = 1.39$ for the $^{16}O + ^{76}Ge$ and $^{18}O + ^{74}Ge$ reaction, respectively. The parameter V_{CBRED} describes the percentage reduction of the effective barrier by 3.78% of V_{CB} for the $^{16}O + ^{76}Ge$ reaction and 3.88% of V_{CB} for the $^{18}O + ^{74}Ge$ reaction.

For the present reactions, the channel coupling parameter increases from $\lambda = 1.32$ to $\lambda = 1.38$ as one moves from the $^{16}O + ^{70}Ge$ to the $^{16}O + ^{76}Ge$ reaction and is found to have a maximum value of $\lambda = 1.39$ for the $^{18}O + ^{74}Ge$ reaction. The percentage reduction of effective fusion barrier V_{CBRED} also increases from 3.64% of V_{CB} and 3.88% of V_{CB} as one moves from the $^{16}O + ^{70}Ge$ to the $^{18}O + ^{74}Ge$ reaction (see Table III). This indicates that the impacts of channel coupling become more pronounced with an increase of neutron richness in a target. Although the channel coupling effects of projectile and target are not considered explicitly in the SAGBD model and one cannot check out the influences of individual DOF on fusion dynamics of the studied reactions, we are mainly interested to check out the influence of all dominant coupling effects that average out the fusion cross sections. Such behavior of the fusion cross section is inferred from the present calculations. Thus, the present method is not as good as the coupled channel approach but cumulative effects of dominant channel coupling can be reasonably recovered by the model calculations.

C. Coupled channel analysis of the fusion cross-section data

In order to strengthen the outcomes of the SAGBD model, the fusion dynamics of chosen reactions are also analyzed by using the coupled channel approach. The coupled channel calculations of the studied reactions are carried out by using the coupled channel code CCFULL [58]. The code CCFULL entertains coupling to all orders and includes the finite excitation energies. In this code, the coupled channel equations are solved by using the ingoing wave boundary conditions (IWBC) and isocentrifugal approximations. Both of these approximations are valid for the heavy-ion fusion reactions. In coupled channel calculations, the couplings to low lying inelastic surface excitations like 2^+ and 3^- vibrational states of colliding systems and the neutron transfer channels are entertained. The deformation parameters for quadrupole and octupole vibrational states and their corresponding excitation energies of the colliding nuclei are taken from Refs. [13,23,26,32]. For the coupled channel calculations, the depth, diffuseness, and range of the Woods-Saxon potential are taken as150 MeV, 0.68 fm, and 1.11 fm, respectively. All these parameters are used in CCFULL as input for the nuclear potential for estimating the fusion cross section for reactions under consideration. The details of coupled channel calculations for the studied reactions are presented in Figs. 11 and 12.

Morton *et al.* [64] pointed out the weak influences of the low-lying quantum states of the ^{16}O isotope in the fusion dynamics of $^{16}O + ^{208}Pb$ and the presence of strong channel couplings; it is very difficult to identify the significance of such weak couplings. The Ge isotope lies in the region of

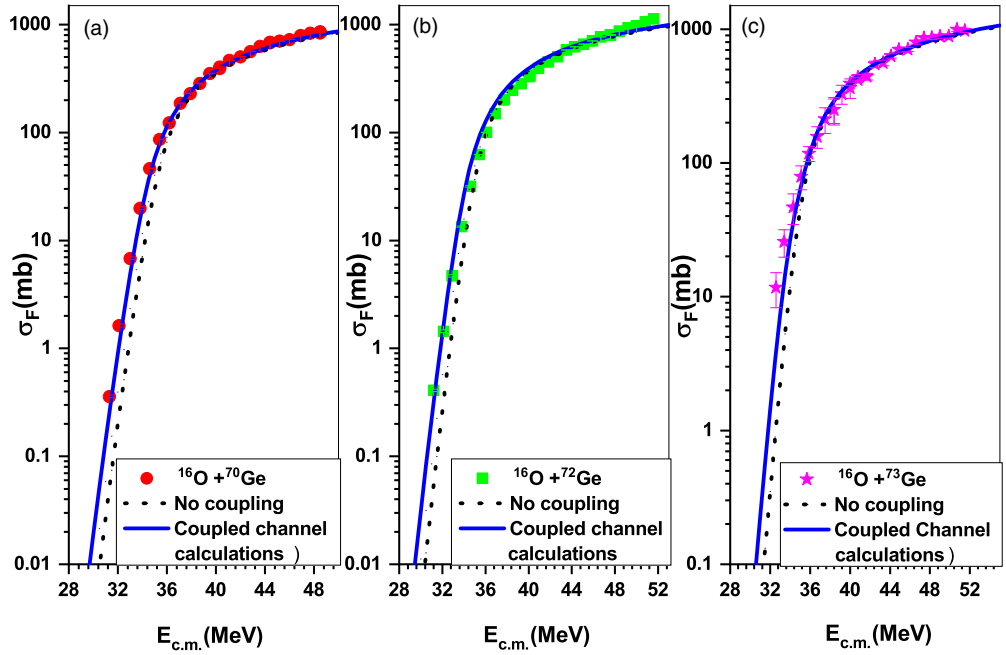

FIG. 11. The fusion excitation functions of $^{16}O + ^{70,72,73}Ge$ reactions obtained by using the coupled channel method. The calculated fusion cross sections are compared with the available experimental data taken from Ref. [13].

weak coupling and one can unambiguously identify the contribution of the collective excitations of the ^{16}O isotope in the fusion reaction dynamics. In case of $^{16}O + ^{70,72}Ge$ reactions, the vibrational states of the colliding systems are dominant. For the $^{16}O + ^{70}Ge$ reaction, due to the doubly magic nature of the projectile it facilitates the couplings to low lying inelastic surface excitations. However, due to high excitation energies of low-lying inelastic surface excitations, the projectile participates weakly in the fusion process. In contrast, the inelastic surface excitations of the target isotope play a crucial role in the enhancement of the sub-barrier fusion cross section of the chosen reactions with reference to the expectations of the 1-DBPM. In the coupled channel description, no-coupling calculations, wherein the fusion partners are taken as inert systems, quantitatively fail to explain the observed fusion enhancement particularly at sub-barrier energies. However,

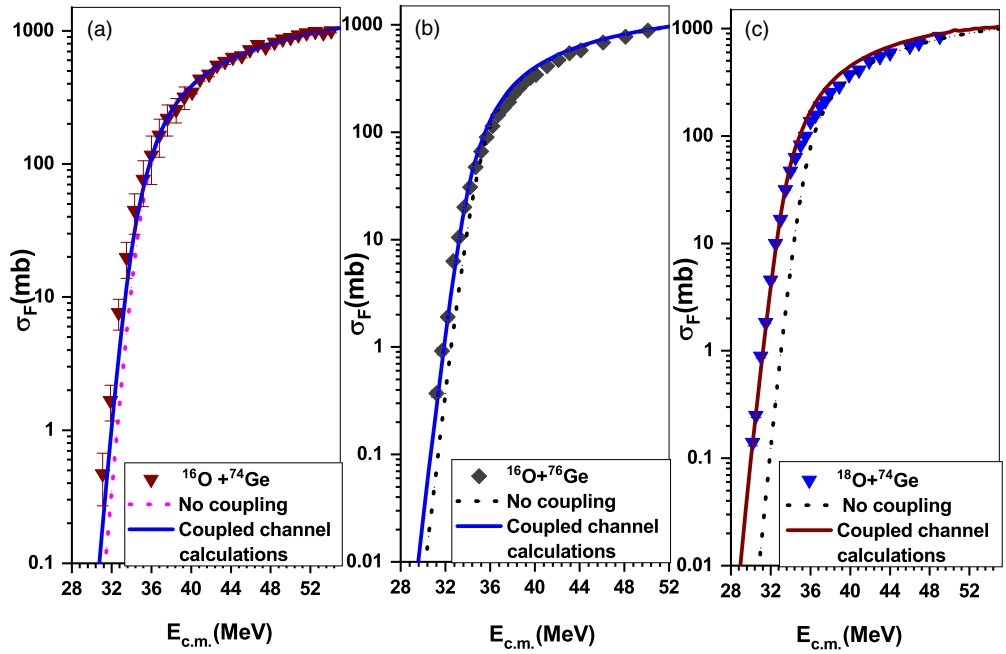

FIG. 12. Same as Fig. 11 but for $^{16}O + ^{74,76}Ge$ and $^{18}O + ^{74}Ge$ reactions. The calculated fusion cross sections are compared with the available experimental data taken from Refs. [13,23].

the fusion data at above barrier energies can be reasonably recovered by such a coupling scheme. The addition of the single phonon 2^+ vibrational state of the target enhances the magnitude of the fusion excitation functions in below barrier energy regions but is unable to recover the required order of magnitude of the observed sub-barrier fusion enhancement. This clearly suggests the possible influences of the more intrinsic channels. The consideration of single phonon 2^+ and 3^- vibrational states of the target along with their mutual couplings significantly improves the calculated results. However, the target degrees of freedom are not sufficient to explain the fusion data, so it is necessary to add the projectile excitations to obtain consistent fits with the experimental data. To overcome deviations between theoretical predictions and the sub-barrier fusion data, the projectile excitations are included in the coupled channel calculations. Therefore, the couplings to the single phonon 2^+ vibrational state of the projectile and the single phonon 2^+ and 3^- vibrational states of the target along with their mutual couplings quantitatively recover the fusion dynamics of the $^{16}O + ^{70}Ge$ reaction as shown in Fig. 11(a). A similar coupling scheme has been tested for the $^{16}O + ^{72}Ge$ reaction. In the case of the $^{16}O + ^{72}Ge$ reaction, the couplings to the single phonon 2^+ vibrational state of the projectile and the single phonon 2^+ and 3^- vibrational states of the target along with their mutual couplings consistently explain the fusion dynamics of chosen reactions at near and below barrier energies as depicted in Fig. 11(b).

The ^{73}Ge nucleus possesses a larger number of odd spin states at excitation energies of 0.013, 0.069, 0.499, and 0.826 MeV. Newton *et al.* [65] pointed out the importance of the odd-*A* spin states of the ^{35}Cl isotope. The odd-*A* spin states were combined in quadrature and considered in the coupled channel description for extracting their possible impacts on fusion dynamics of the $^{35}Cl + ^{92}Zr$ reaction. As we are mainly interested to check out the coupling effects due to dominant states rather than the individual angular momentum distribution of all odd-*A* states, so all odd-*A* excited states of the ^{73}Ge isotope are added in quadrature for the present coupled channel analysis. In other words, the cumulative effects of all the odd spin states of the ^{73}Ge isotope are included in quadrature, which in turn are considered in the coupled channel description for the explanation of the fusion dynamics of the $^{16}O + ^{73}Ge$ reaction. The coupled channel calculations obtained by entertaining the odd-*A* spin states enhance the magnitude of calculated fusion cross sections and hence appropriately reproduced the fusion data of the chosen reaction in the entire energy range around the Coulomb barrier as depicted in Fig. 11(c).

For the $^{16}O + ^{74}Ge$ reaction in the no-coupling case, the projectile and target are considered as inert systems and such calculations remain sufficiently smaller than that of fusion data of the chosen reaction. But in the above barrier energy regions, no-coupling calculations adequately explored the fusion data points. The coupling to the single phonon 2^+ vibrational state of the target results in substantially larger fusion enhancement at sub-barrier energies over no-coupling calculations but these are unable to address the experimental data consistently. This highlights the need for more intrinsic channels in the coupled channel description. The considerations of the single phonon 2^+ and 3^- vibrational states of the target along with their mutual couplings like $2^+ \otimes 3^-$ improve the theoretical results. However, the discrepancies between calculated results and experimental data still demand the inclusion of more intrinsic channels. To overcome such deviations, the projectile excitations are entertained in the coupled channel approach. In this sense, the couplings to the single phonon 2^+ vibrational state of the projectile, single phonon 2^+ and 3^- vibrational states of the target, along with their mutual couplings such as $2^+ \otimes 3^-$ are incorporated in model calculations. Such calculations quantitatively reproduced sub-barrier fusion enhancement of the $^{16}O + ^{74}Ge$ reaction around the Coulomb barrier as shown in Fig. 12(a). This clearly identifies that $^{70,72,73}Ge$ isotopes are spherical in their ground state and low-lying inelastic surface excitations of the target are dominant modes of coupling.

For the $^{16}O + ^{76}Ge$ reaction, no-coupling calculations predict a significantly smaller fusion cross section in sub-barrier energy regions, while the above barrier fusion data are approximately recovered by such theoretical predictions. The discrepancies between the no-coupling scheme and the experimental data can be understood in terms of the vibrational couplings associated with the colliding systems. The inclusion of the vibrational states like single phonon 2^+ or 3^- vibrational states in the target leads to larger sub-barrier fusion enhancements with reference to the no-coupling scheme. But these calculations are unable to recover the observed fusion data of a given reaction. The additions of single phonon vibrational states of quadrupole and octupole types and their mutual couplings improve the results slightly but still fail to explain the fusion data in the sub-barrier energy region. To address the fusion dynamics of the chosen system, the 2^+ vibrational state of the projectile as well as the rotational states of the target up to 6^+ ground-state rotational band for ^{76}Ge are entertained in the calculations. The so obtained results shift towards the experimental data at sub-barrier energies, but more intrinsic channels are needed for the adequate description of fusion data of the studied system. As it is already mentioned in the literature, the ^{76}Ge isotope is statistically deformed and possesses higher-order deformation in the ground state. Therefore, incorporating the $\beta_2 = 0.27$ and $\beta_4 = 0.02$ along with the projectile excitations reasonably reproduces the sub-barrier fusion dynamics of $^{16}O + ^{76}Ge$ reaction as depicted in Fig. 12(b).

In the case of the $^{18}O + ^{74}Ge$ reaction, the projectile being spherical in nature exhibits low lying 2^+ and 3^- vibrational states. Due to low excitation energies and large coupling strength, the projectile is expected to be involved actively in the fusion of the $^{18}O + ^{74}Ge$ reaction. The inclusion of the single phonon 2^+ vibrational state or the 3^- vibrational state in the target nucleus is unable to give a close agreement between theoretical results and the experimental data. The coupling to single phonon 2^+ and 3^- vibrational states along with their mutual couplings in the target results in a substantially larger fusion enhancement at sub-barrier energies but fails to recover the observed sub-barrier fusion enhancement. This is an indication of adding more intrinsic channels for addressing the experimental data in below barrier energy regions. The coupling to the single phonon 2^+ vibrational state in the projectile

and the one phonon 2^+ and 3^- vibrational state in the target along with their mutual couplings are sufficient to recover the fusion data of the $^{18}O + ^{74}Ge$ reaction. In addition, the chosen reaction offers the possibility of two neutron transfer channels with positive ground state Q value and it is quite interesting to check out the influence of transfer couplings on the fusion process. The two-neutron transfer channel with a positive Q value of 3.75 MeV and coupling strength of 0.7 MeV for the transfer channel is considered in the coupled channel analysis. The transfer coupling strength can be adjusted in order to get good fits to above the barrier data of fusion and transfer coupling strength $F_t = 0.7$ MeV gives the best fit to the experimental data. The inclusion of two neutron transfer channels along with inelastic surface excitations of the target nucleus ^{74}Ge enhances the magnitude of the fusion cross sections but slightly overestimates the fusion data at below barrier energies while it underpredicts the data in the above barrier energy regions. This suggests that the neutron transfer channels impart a small contribution to the fusion dynamics of the $^{18}O + ^{74}Ge$ reaction and hence the fusion dynamics of the chosen system is dominated by the collective excitations of collision partners as depicted in Fig. 12(c). For the chosen reaction, the outcomes of the SAGBD model and coupled channel code CCFULL are almost similar, which clearly indicates that the SAGBD model intrinsically considers the various channel coupling effects associated with the colliding nuclei.

D. χ^2 analysis for the fusion cross-section data

In order to judge the accuracy of output results obtained by the adopted model, the χ^2 analysis is performed for the SAGBD model calculations. The goodness of fit for theoretical outcomes can be examined by χ^2 analysis. The formula for χ^2 analysis is given by the following relation [13,22,41]:

$$\chi^2 = \frac{1}{N}\sum_{i=1}^{N}\left[\frac{\{\sigma_{ex}(E_{c.m.}) - \sigma_{th}(E_{c.m.})\}^2}{\sigma_{th}(E_{c.m.})}\right]$$

wherein N represents the total experimental data points in each system and σ_{th} and σ_{ex} are the model and experimentally measured cross sections, respectively.

The deviations of the theoretical cross section from the experimental cross section have been measured via χ^2 analysis for various systems studied under consideration. The present χ^2 analysis also includes the experimental uncertainties of the data. The present χ^2 values deduced for the SAGBD model calculations are listed in Table IV. The calculated values of χ^2 for different systems $^{16}O + ^{70}Ge$, $^{16}O + ^{72}Ge$, $^{16}O + ^{73}Ge$, $^{16}O + ^{74}Ge$, $^{16}O + ^{76}Ge$, and $^{18}O + ^{74}Ge$ are found to be 1.54, 4.23, 2.21, 2.48, 1.43, and 2.36, respectively. The present χ^2 values are consistent with that of the coupled channel approach and thus point towards the accuracy of the adopted model.

E. Reduced scale analysis of fusion data

Figure 13(a) shows the comparison of fusion cross-section data for $^{16}O + ^{70,72,73,74,76}Ge$ reactions in a reduced scale which indicates that the fusion enhancements at sub-barrier energies increase with an increase in neutron

TABLE IV. χ^2 values for $^{16}O + ^{70,72,72,74,76}Ge$ and $^{18}O + ^{74}Ge$ obtained by using the SAGBD model along with corresponding coupled channel values [13,23].

System	χ^2 values (SAGBD model)	χ^2 values (coupled channel approach)
$^{16}O + ^{70}Ge$	1.54	1.50
$^{16}O + ^{72}Ge$	4.23	3.70
$^{16}O + ^{73}Ge$	2.21	1.80
$^{16}O + ^{74}Ge$	2.48	3.50
$^{16}O + ^{76}Ge$	1.43	1.50
$^{18}O + ^{74}Ge$	2.36	2.70

richness, but such effects are very weak. In the case of $^{16}O + ^{144,148,150,152,154}Sm$ reactions, with an increase of neutron richness, the target gradually changes from a spherical ($^{144,148}Sm$) to a statically deformed ($^{152,154}Sm$) shape and shows strong target isotopic dependence of fusion cross sections [22,66–69]. Although there are shape transition effects in $^{70,72,73,74,76}Ge$ isotopes, the fusion dynamics of $^{16}O + ^{70,72,73,74,76}Ge$ reactions do not show strong target isotopic dependence of sub-barrier fusion enhancement as observed for $^{16}O + ^{144,148,150,152,154}Sm$ reactions. This portrays that Ge isotopes lie in the region of weak deformations, henceforth the influences of target deformations are not so pronounced as found in the case of Sm isotopes.

Further to single out the contribution of neutron transfer channels with positive Q values, the fusion dynamics of $^{16}O + ^{76}Ge$ and $^{18}O + ^{74}Ge$ reactions are compared with each other and the results of the comparison are shown in Fig. 13(b). In the case of $^{16}O + ^{76}Ge$ the effects of the neutron transfer channel are suppressed due to the negative ground state Q values while the $^{18}O + ^{74}Ge$ reaction facilitates a 2 n-pickup channel with a positive Q value. The comparison of these data clearly indicates that fusion data of both reactions overlap with each other in near and above barrier energy regions, which, in turn, reflects the absence of strong

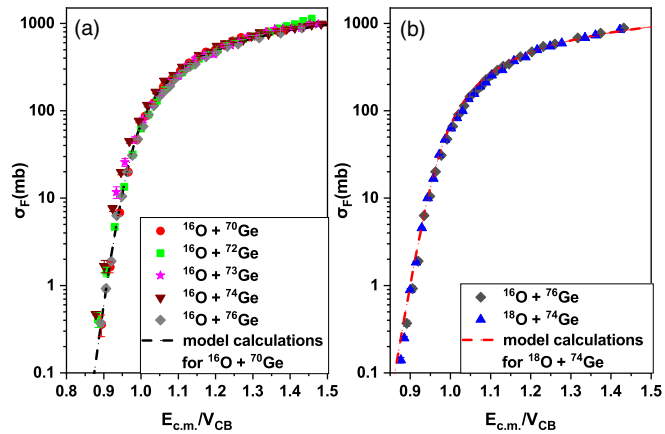

FIG. 13. Fusion cross-section data for $^{16}O + ^{70,72,73,74,76}Ge$ systems (a) and $^{16}O + ^{76}Ge$ and $^{18}O + ^{74}Ge$ systems (b) are compared in reduced scale. The experimental data of chosen reactions are taken from Refs. [13,23].

fusion enhancement of the $^{18}O+^{74}Ge$ reaction relative to the $^{16}O+^{76}Ge$ reaction. This further indicates that the neutron transfer channel has a weak influence on the fusion dynamics of the $^{18}O+^{74}Ge$ reaction. Although there is an absence of strong fusion enhancement of $^{18}O+^{74}Ge$ relative to $^{16}O+^{76}Ge$ reaction, the role of neutron transfer channels cannot be ruled out completely. One can also check out the contribution of entrance channel mass asymmetry on the fusion process of the $^{16}O+^{76}Ge$ and $^{18}O+^{74}Ge$ reactions. Both of these reactions have different entrance channels but form the same compound nucleus (^{92}Zr). In the literature [51,70–72], it has been found that larger entrance channel mass symmetry favors the fusion process and results in a larger fusion cross section at sub-barrier energies. Therefore, the entrance channel mass symmetry may affect the fusion dynamics of these reactions, and its value for both reactions is given below:

$$\eta = \left|\frac{A_1 - A_2}{A_1 + A_2}\right| = \left|\frac{16-76}{16+76}\right| = \frac{60}{92}$$
$$= 0.65 \quad \text{for the } ^{16}O+^{76}Ge \text{ reaction},$$
$$\eta = \left|\frac{A_1 - A_2}{A_1 + A_2}\right| = \left|\frac{18-74}{18+74}\right| = \frac{56}{92}$$
$$= 0.61 \text{ for the } ^{18}O+^{74}Ge \text{ reaction}.$$

The entrance channel mass symmetry is larger for the $^{16}O+^{76}Ge$ reaction relative to the $^{18}O+^{74}Ge$ reaction and due to this the $^{16}O+^{76}Ge$ reaction may gain some additional sub-barrier fusion enhancements. The entrance channel mass symmetry of the $^{18}O+^{74}Ge$ reaction is smaller but the effects of the neutron transfer channel come into the picture and the influences of these factors may be smeared with each other. Consequently, the fusion enhancement of the $^{18}O+^{74}Ge$ reaction is almost same as that of the $^{16}O+^{76}Ge$ reaction. A closer look at the lowest energy data of the $^{18}O+^{74}Ge$ reaction clearly suggests the larger sub-barrier fusion enhancement for $^{18}O+^{74}Ge$ relative to the $^{16}O+^{76}Ge$ reaction and such effects can only be attributed to two neutron pickup channels with positive Q value. Henning *et al.* [73] emphasized that the conclusions regarding the impacts of transfer channels become clear if one deals with the optimum Q value rather than the Q value for transfer channels. This is because in some cases, the Q value is positive while its corresponding optimum Q value is negative and such a transfer channel weakly affects the fusion process. However, in some cases, where both the Q value and the optimum Q value are positive, the fusion cross section shows strong correlation with the neutron transfer channels as observed for $^{40}Ca+^{96}Zr$ [74], $^{32}Ca+^{96}Zr$ [75], and $^{28}Si+^{96}Zr$ [57,65,76] reactions. By using the quantum diffusion approach, Sargsyan *et al.* [77] analyzed the role of neutron transfer channels on the fusion process. The authors suggested that if the deformation of colliding pairs remains the same or unchanged or decreases after neutron transfer then there are weak influences of the nucleon transfer channel on the fusion process. On the other hand, if the deformation increases after neutron transfer, then there will be a strong fusion enhancement of the fusion cross section at near and sub-barrier energies. In the $^{18}O+^{74}Ge$ reaction, the transfer of two neutrons from the projectile to the target changes ^{74}Ge to ^{76}Ge and the deformation of ^{76}Ge remains ($\beta_2 = 0.27$) smaller in magnitude relative to that of the ^{74}Ge isotope ($\beta_2 = 0.29$). This decrease in deformation compensates the effects of the neutron transfer channel in the fusion process and consequently it reflects a weak dependence of the fusion cross section on the neutron transfer channel. The similar behavior of the fusion cross section is also reflected in the present calculations.

IV. CONCLUSION

In this article, the sensitivity of fusion cross sections and experimental barrier distributions is investigated for $^{16}O+^{70,72,73,74,76}Ge$ and $^{18}O+^{74}Ge$ reactions at energies near and below the Coulomb barrier. The theoretical predictions suggest that the fusion cross sections and barrier distribution are extremely sensitive to the choice of nuclear potential as well as the potential parameters. Theoretical calculations based on the one-dimensional Wong formula strongly underpredict the experimental data. This points out the importance of the channel coupling effects that may be responsible for the observed sub-barrier fusion enhancements. Without considering the channel coupling effects, one cannot reproduce the experimental data of studied systems particularly in below barrier energy regions. However, calculations based on the SAGBD model intrinsically include the multidimensional character of tunneling effects and consequently incorporate the contributions from the dominant channel in terms of channel coupling parameter λ. In the present model, a larger value of λ indicates the greater effects of nuclear structure of participating nuclei on the fusion process. Thus λ is related directly or indirectly with the various channel coupling effects that are responsible for sub-barrier fusion enhancement with reference to the estimations of 1-DBPM. For $^{16}O+^{70,72,73,74,76}Ge$ and $^{18}O+^{74}Ge$ reactions, the channel coupling parameter λ increases from 1.32 to 1.38 as one moves from ^{70}Ge to ^{76}Ge, which clearly indicates that there are shape transition effects from spherical symmetry to prolate deformed shape. In addition, the V_{CBRED} increases from 3.64% of V_{CB} for $^{16}O+^{76}Ge$ to 3.78% of V_{CB} for the $^{16}O+^{76}Ge$ reaction which is a clear signature of the shape transition effects in the target isotope with an increase in neutron richness. The values of λ and V_{CBRED} are found to be largest for $^{18}O+^{74}Ge$ reaction and hence suggest the combined effects of collective excitations and neutron transfer channel for this system. The SAGBD calculations reasonably reproduced the fusion cross sections and experimental barrier distributions of $^{16}O+^{70,72,73,74,76}Ge$ and $^{18}O+^{74}Ge$ reactions and thus intimate the adequacies of the symmetric Gaussian type of weight function adopted for the present case.

For the studied reactions, the coupled channel calculations that are carried out by using the code CCFULL and these calculations unambiguously indicate that the couplings to low-lying vibrational states (such as 2^+ and 3^-) of the target are important for $^{16}O+^{70,72,73,74}Ge$ reactions. For $^{16}O+^{70,72,73,74}Ge$ reactions, the consideration of vibrational couplings is sufficient to account for the observed sub-barrier fusion enhancement of these reactions. For the $^{16}O+^{76}Ge$ reaction, the couplings to rotational states along with higher-

order deformation such as β_4 are essentially required for the complete addressal of the fusion enhancement at below barrier energies. In the case of the $^{18}O + ^{74}Ge$ reaction, the inclusion of low-lying vibrational states like 2^+ and 3^- vibrational states of the projectile and the target is primarily required to reproduce the sub-barrier fusion enhancement. The coupling to the $2n$-transfer channel weakly affects the sub-barrier fusion enhancement. Furthermore, the $^{18}O + ^{74}Ge$ reaction is less mass asymmetric in the entrance channel while the $^{16}O + ^{76}Ge$ reaction has a larger entrance channel mass asymmetry. Therefore, the effects of entrance channel mass asymmetry and the neutron transfer channel may be compensated with each other for the $^{18}O + ^{74}Ge$ system. The transfer of two neutrons for the $^{18}O + ^{74}Ge$ reaction decreases the deformation, and thus the effects of the PQNT channel turn out to be smaller for this system. Such behaviors are consistent with the findings of Sargsyan *et al.* [77]. Further, the χ^2 values obtained for the SAGBD model calculations are also comparable with that based on the coupled channel approach.

ACKNOWLEDGMENT

Vijay is sincerely thankful to the Council of Scientific & Industrial Research (CSIR), New Delhi, India for providing a CSIR-JRF fellowship under Grant No. 09/1307(0001)/2020-EMR-I.

[1] A. B. Balantekin and N. Takigawa, Rev. Mod. Phys. **70**, 77 (1998).
[2] B. B. Back, H. Esbensen, C. L. Jiang, and K. E. Rehm, Rev. Mod. Phys. **86**, 317 (2014).
[3] M. Dasgupta, D. J. Hinde, N. Rowley, and A. M. Stefanini, Annu. Rev. Nucl. Part. Sci. **48**, 401 (1998).
[4] M. S. Gautam, Mod. Phys. Lett. A **30**, 1550013 (2015).
[5] N. Keeley, R. Raabe, N. Alamanos, and J. L. Sida, Prog. Part. Nucl. Phys. **59**, 579 (2007).
[6] C. H. Dasso, S. Landowne, and A. Winther, Nucl. Phys. A **405**, 381 (1983).
[7] C. H. Dasso, S. Landowne, and A. Winther, Nucl. Phys. A **407**, 221 (1983).
[8] K. Hagino, N. Takigawa, and A. B. Balantekin, Phys. Rev. C **56**, 2104 (1997).
[9] M. S. Gautam, K. Vinod, and H. Kumar, Braz. J. Phys. **47** (2017) 461.
[10] A. O. Caldera and A. J. Leggett, Phys. Rev. Lett. **46**, 211 (1981).
[11] P. R. S. Gomes *et al.*, Phys. Rev. C **49**, 245 (1994).
[12] M. S. Gautam, Indian J. Phys. **90**, 335 (2016).
[13] E. F. Aguilera, J. J. Kolata, and R. J. Tighe, Phys. Rev. C **52**, 3103 (1995).
[14] M. S. Gautam, Nucl. Phys. A **933**, 272 (2015).
[15] P. H. Stelson, Phys. Lett. B **205**, 190 (1988).
[16] M. S. Gautam, H. Khatri, and K. Vinod, Nucl. Phys. A **984**, 9 (2019).
[17] J. R. Leigh *et al.*, Phys. Rev. C **52**, 3151 (1995).
[18] M. Dasgupta, D. J. Hinde, A. Diaz-Torres, B. Bouriquet, Catherine I. Low, G. J. Milburn, and J. O. Newton, Phys. Rev. Lett. **99**, 192701 (2007).
[19] K. Hagino and N. Rowley, Phys. Rev. C **69**, 054610 (2004).
[20] N. Rowley, G. R. Satchler, and P. H. Stelson, Phys. Lett. B **254**, 25 (1991).
[21] L. F. Canto, P. R. S. Gomes, R. Donangelo, and M. S. Hussein, Phys. Rep. **424**, 1 (2006).
[22] E. F. Aguilera, J. J. Vega, J. J. Kolata, A. Morsad, R. G. Tighe, and X. J. Kong, Phys. Rev. C **41**, 910 (1990).
[23] H. M. Jia, C. J. Lin, F. Yang, X. X. Xu, H. Q. Zhang, Z. H. Liu, L. Yang, S. T. Zhang, P. F. Bao, and L. J. Sun, Phys. Rev. C **86**, 044621 (2012).
[24] D. M. Brink and U. Smilansky, Nucl. Phys. A **405**, 301 (1983).
[25] D. L. Hill and J. A. Wheeler, Phys. Rev. **89**, 1102 (1953).
[26] M. S. Gautam, H. Khatri, and K. Vinod, Int. J. Mod. Phys. E **28**, 1950006 (2019).
[27] K. Washiyama, K. Hagino, and M. Dasgupta, Phys. Rev. C **73**, 034607 (2006).
[28] M. S. Gautam, Chin. Phys. C **39**, 114102 (2015).
[29] M. S. Gautam, Can. J. Phys. **93**, 1343 (2015).
[30] M. S. Gautam, Phys. Rev. C **90**, 024620 (2014).
[31] J. O. Newton, R. D. Butt, M. Dasgupta, D. J. Hinde, I. I. Gontchar, C. R. Morton, and K. Hagino, Phys. Rev. C **70**, 024605 (2004).
[32] M. S. Gautam, Phys. Scr. **90**, 055301 (2015).
[33] A. Mukherjee, D. J. Hinde, M. Dasgupta, K. Hagino, J. O. Newton, and R. D. Butt, Phys. Rev. C **75**, 044608 (2007).
[34] J. F. Niello, C. H. Dasso, and S. Landowne, Comput. Phys. Commun. **54**, 409 (1989).
[35] M. Liu, N. Wang, Z. Li, X. Wu, and E. Zhao, Nucl. Phys. A **768**, 80 (2006).
[36] V. Zanganeh, R. Gharaei, and A. M. Izadpanah, Nucl. Phys. A **992**, 121637 (2019).
[37] K. Swiek-Wilczyńska, E. Siemaszko, and J. Wilczyński, Acta Phys. Pol. B **33**, 451 (2002).
[38] K. Swiek-Wilczyńska and J. Wilczyński, Phys. Rev. C **69**, 024611 (2004).
[39] C. L. Jiang, K. E. Rehm, B. B. Back, A. M. Stefanini, and G. Montagnoli, Eur. Phys. J. A **54**, 218 (2018).
[40] C. Y. Wong, Phys. Rev. Lett. **31**, 766 (1973).
[41] E. Martinez-Quiroz, E. F. Aguilera, J. J. Kolata, and M. Zahar, Phys. Rev. C **63**, 054611 (2001).
[42] D. W. Grissmer, R. Beyer, R. P. Scharenberg, G. Schilling, J. A. Thomson, and J. W. Tippie, Nucl. Phys. A **196**, 216 (1972).
[43] M. E. Cobern, N. Lisbona, and M. C. Mermaz, Phys. Rev. C **13**, 674 (1976).
[44] M. E. Cobern, M. C. Lemaire, K. S. Low, M. C. Mermaz, H. Sztark, T. Udagawa, and T. Tamura, Phys. Rev. C **13**, 1200 (1976).
[45] R. Lecomte, G. Kajrys, S. Landsberger, P. Paradis, and S. Monaro, Phys. Rev. C **25**, 2812 (1982).
[46] S. Sen, S. E. Darden, R. C. Luhn, N. O. Gaiser, G. Murillo, and J. Ramirez, Phys. Rev. C **31**, 787 (1985).
[47] F. Ballester, E. Casal, and J. B. A. England, Nucl. Phys. A **490**, 227 (1988).
[48] D. Goutte, in *Proceedings of the International Conference on Nuclear Shape*, edited by F. Dykstra, D. Goutte, J. Sauvage, and M. Vergnes (World Scientific, Singapore, 1988), p. 36.
[49] M. Singh, Sukhvinder, and R. Kharab, Nucl. Phys. A **897**, 198 (2013).

[50] M. S. Gautam, Rev. Mex. Fis. **62**, 398 (2016).
[51] H. Esbensen, Phys. Rev. C **68**, 034604 (2003).
[52] H. Esbensen, Phys. Rev. C **72**, 054607 (2005).
[53] Muhammad Zamrun F., Zakarya Mohamed Mohamed Mahmoud, N. Takigawa, and K. Hagino, Phys. Rev. C **81**, 044609 (2010).
[54] T. H. Curtis, H. F. Lutz, and W. Bartolin, Phys. Rev. C **1**, 1418 (1970).
[55] J. Jabbour, L. H. Rosier, E. I. Obiajunwa, and Ramstein, Nucl. Phys. A **500**, 356 (1989).
[56] G. Szaloky, L. A. Montestruque, M. C. Cobian-Rozak, and S. E. Darden, Phys. Rev. C **18**, 750 (1978).
[57] M. S. Gautam, S. Duhan, R. P. Chahal, H. Khatri, S. B. Kuhar, and K. Vinod, Phys. Rev. C **102**, 014614 (2020).
[58] K. Hagino, N. Rowley, and A. T. Kruppa, Comput. Phys. Commun. **123**, 143 (1999).
[59] R. M. Anjos *et al.*, Phys. Rev. C **42**, 354 (1990).
[60] D. M. Brink, *Semi-Classical Methods for Nucleus-Nucleus Scattering* (Cambridge University, Cambridge, England, 1985).
[61] C. Y. Wong, Phys. Lett. B **42**, 186 (1972).
[62] J. Dobaczewski, W. Nazarewicz, J. Skalski, and T. Werner, Phys. Rev. Lett. **60**, 2254 (1988).
[63] M. M. Sharma, M. A. Nagarajan, and P. Ring, Phys. Lett. B **312**, 377 (1993).
[64] C. R. Morton *et al.*, Phys. Rev. Lett. **72**, 4074 (1994).
[65] J. O. Newton, C. R. Morton, M. Dasgupta, J. R. Leigh, J. C. Mein, D. J. Hinde, H. Timmers, and K. Hagino, Phys. Rev. C **64**, 064608 (2001).
[66] R. Lecomte, M. Irshad, S. Landsberger, P. Paradis, and S. Monaro, Phys. Rev. C **22**, 1530 (1980); R. Lecomte, M. Irshad, S. Landsberger, G. Kajrys, and S. Monaro, *ibid.***22**, 2420 (1980).
[67] R. G. Stokstad, Y. Eisen, S. Kaplanis, D. Pelte, U. Smilansky, and I. Tserruya, Phys. Rev. C **21**, 2427 (1980).
[68] D. E. DiGregorio *et al.*, Phys. Rev. C **39**, 516 (1989).
[69] E. F. Aguilera, Rev. Mex. Fis. **38**, 63 (1992).
[70] M. S. Gautam, Commun. Theor. Phys. **64**, 710 (2015).
[71] M. S. Gautam, Rom. Rep. Phys. **68**, 1035 (2016).
[72] M. S. Gautam, Chin. J. Phys. **54**, 86 (2016).
[73] W. Henning, F. L. H. Wolfs, J. P. Schiffer, and K. E. Rehm, Phys. Rev. Lett. **58**, 318 (1987).
[74] A. M. Stefanini *et al.*, Phys. Lett. B **728**, 639 (2014).
[75] H. Q. Zhang *et al.*, Phys. Rev. C **82**, 054609 (2010).
[76] Khushboo *et al.*, Phys. Rev. C **96**, 014614 (2017).
[77] V. V. Sargsyan, G. G. Adamian, N. V. Antonenko, W. Scheid, and H. Q. Zhang, Eur. Phys. J. A **49**, 54 (2013).